Influence of 3D-printed circular patterns on the tensile properties of tulle fabric

DOI: 10.35530/IT.077.05.20266

IULIANA STREBA
ARINA SEUL
AURA MIHAI

ANTONELA CURTEZA
MARIANA COSTEA
RAMONA BUDEANU

ABSTRACT – REZUMAT

Influence of 3D-printed circular patterns on the tensile properties of tulle fabric

This study investigates the influence of 3D printing on the tensile mechanical behaviour of tulle, a thin, mesh-like textile commonly used in clothing and technical applications. Four 3D printing geometries were analysed: small and large circles, arranged either aligned or staggered, applied to the surface of the tulle through fused deposition modelling (FDM). Tensile tests were conducted according to ISO 1421:2016, with adaptations required by the textile-polymer composite structure. Maximum force, elongation at break, specific strength, and Young's modulus were evaluated and compared to unprinted control samples. The results show that all printed geometries significantly increase tensile strength compared to plain tulle. At the same time, elongation at break decreased, and the material stiffened with increasing print size and density. The paper highlights the potential of 3D printing to customise and optimise the mechanical properties of thin textiles, opening new directions in the design of flexible hybrid materials.

Keywords: *3D printing on tulle fabric, tensile properties, additive manufacturing, fused deposition modelling (FDM), PLA printed patterns*

Influența modelelor circulare imprimate 3D asupra proprietăților de tracțiune ale țesătură de tip tul

Acest studiu investighează influența imprimării 3D asupra comportamentului mecanic la tracțiune al tulului, un material textil subțire, asemănător unei plase, utilizat în mod obișnuit în îmbrăcăminte și aplicații tehnice. Au fost analizate patru geometrii de imprimare 3D: cercuri mici și mari, aranjate fie aliniate, fie decalate, aplicate pe suprafața tulului cu ajutorul modelării prin depunere de material topit (FDM). Testele de tracțiune au fost efectuate conform ISO 1421:2016, cu adaptările necesare structurii compozite textil-polimer. Au fost evaluate forța maximă, alungirea la rupere, rezistența specifică și modulul lui Young, comparativ cu probele de control neimprimate. Rezultatele arată că toate geometriile imprimate cresc semnificativ rezistența la tracțiune în comparație cu tulul simplu. În același timp, alungirea la rupere a scăzut, iar materialul s-a rigidizat odată cu creșterea dimensiunii și densității imprimării. Lucrarea evidențiază potențialul imprimării 3D de a personaliza și optimiza proprietățile mecanice ale textilelor subțiri, deschizând noi direcții în proiectarea materialelor hibride flexibile.

Cuvinte-cheie*: imprimare 3D pe țesătură de tip tul, proprietăți de tracțiune, fabricație aditivă, modelare prin depunere de material topit (FDM), modele imprimate cu PLA*

INTRODUCTION

Additive manufacturing (AM) has transformed material production over the past two decades, expanding its influence from industrial prototyping to advanced fields such as biomedical engineering, aerospace, automotive design, and, increasingly, textile engineering [1]. Unlike conventional subtractive or formative techniques, AM enables the fabrication of complex three-dimensional structures through controlled material deposition, offering greater manufacturing freedom, sustainability advantages, and unprecedented opportunities for customisation [2]. As 3D printing technologies mature and diversify, their integration with textiles has become one of the most dynamic research frontiers, giving rise to what is now commonly termed Textile Additive Manufacturing (TAM).

TAM comprises two primary research pathways: (1) direct printing onto textile substrates and (2) additive manufacturing of textile-like structures that mimic or extend the behaviour of conventional fabrics [1]. In the first pathway, a thermoplastic filament – commonly PLA, TPU, or PA6.6 – is deposited directly onto a fabric, creating hybrid textile-polymer composites with modified mechanical, aesthetic, or functional performance [3, 4]. The second pathway focuses on designing quasi-textile structures through CAD, assembling unit cells into flexible networks that approximate the drape, elasticity, or deformation mechanisms of woven or knitted textiles [5, 6]. These strategies are reshaping the apparel and wearable technology industries by enabling low-volume, customisable, on-demand production, reducing material

waste and broadening the scope of functional textile design [7, 8].

Recent advancements have highlighted the potential of AM for creating smart textiles by embedding sensors, electrodes, conductive paths, or protective structures directly into textile matrices [9, 10]. In fashion and the arts, designers have embraced 3D printing to create sculptural garments and unique textile surfaces unattainable through traditional techniques [11, 12]. Despite growing interest and experimental activity, fundamental research gaps persist, particularly concerning the mechanical behaviour of textile–polymer hybrids produced via direct printing. Key challenges relate to adhesion control, pattern geometry, substrate porosity, and anisotropic mechanical responses, all of which must be rigorously understood before TAM can mature into a reliable manufacturing paradigm.

The adhesion between the printed polymer and textile substrate is one of the most critical determinants of the mechanical integrity and performance of hybrid materials [3, 4]. Adhesion arises through a combination of mechanical interlocking, thermal bonding, diffusion, and pressure-induced consolidation [13]. The degree of interpenetration of molten filament into the textile pores is influenced by extrusion temperature, print speed, layer height, nozzle-to-fabric Z-distance, and substrate morphology [14, 15]. For example, higher temperatures and lower Z-distances facilitate deeper penetration of molten polymer, improving bond strength but potentially risking fabric deformation or damage [4]. Conversely, insufficient melting or excessive nozzle elevation leads to weak adhesion, delamination, and early mechanical failure.

Fabric pretreatments, such as washing or chemical surface modification, can enhance adhesion by removing surface contaminants or increasing surface energy [4]. Studies comparing cotton, polyester, viscose, and mesh fabrics have shown that adhesion is highly substrate-dependent, with porous structures allowing better mechanical anchoring of polymer filaments [3, 16]. Moreover, the challenge intensifies for ultralight materials such as tulle, whose delicate open mesh structure is highly susceptible to thermal and mechanical disturbances during 3D printing.

Beyond adhesion, geometric parameters of the printed pattern play an essential role in determining the global mechanical performance of textile–polymer composites. Studies have demonstrated that tensile behaviour is strongly influenced by pattern size, orientation, topology, and spatial density [8, 16]. Printed features act as localised stiffening elements, altering load-transfer mechanisms within the fabric and redistributing stresses across the composite structure. For instance, Fajardo et al. (2023) highlighted that linked-unit 3D-printed fabrics exhibit significantly different tensile strengths depending on the type of structural connection, with specific designs acting to delay crack propagation or enhance elongation [5].

Similarly, auxetic structures, which exhibit negative Poisson's ratios, have been shown to provide enhanced energy absorption and resilience, with their behaviour being highly sensitive to unit-cell geometry [6, 17]. These findings underscore the critical interaction between pattern geometry and mechanical performance, reinforcing the need for systematic investigations into how specific geometric features – such as circles, hexagons, grids, or chiral cells interact with textile substrates under tensile loading.

Despite extensive research on textile printing, most studies focus on relatively stable, medium-weight fabrics [4, 8]. In contrast, tulle presents distinct challenges due to its extremely low mass per unit area, high porosity and open-mesh geometry, sensitivity to thermal fluctuations, and pronounced anisotropy that depends on mesh orientation.

In addition to the studies already discussed, earlier foundational work in additive manufacturing, such as Crump's (1989) patent on Fused Deposition Modelling, provides the technological basis for contemporary textile integration [18]. More recent analyses have highlighted the influence of calibration procedures and printing environments on interlayer adhesion and melt flow behaviour. Ghafar et al. (2024) and Gkertzos et al. (2024) demonstrate that ambient temperature, enclosure conditions, and extrusion stability significantly alter polymer viscosity and bonding strength, factors especially relevant when printing on delicate substrates such as tulle [19, 20]. Kozior et al. (2020) further conceptualise adhesion at textile–polymer interfaces by integrating wetting, diffusion, and pressure, offering a theoretical framework that supports the findings of Gorlachova and Mahltig (2021) and extends their applicability to ultralight fabrics [4, 13]. From a textile science perspective, Parajuli et al. (2021) emphasise the historical and structural distinctions among regenerated, synthetic, and natural fibres, underscoring why open mesh fabrics like tulle behave mechanically differently from denser textiles traditionally used in 3D printing experiments [21]. Complementary industrial developments, including Stratasys Ltd.'s (2023) release of textile-oriented AM platforms, indicate a growing movement toward commercial adoption, which further necessitates systematic mechanical investigations such as the present study [22]. Work by Thumsorn et al. (2023) on heat-distribution effects in filament deposition, together with Ren et al.'s (2020) insights into energy absorption in cellular printed geometries, also supports the notion that pattern geometry, even when reduced to simple circular nodes, can drastically modify deformation pathways [23, 24]. Finally, recent research on surface texturing of polymers and on metamaterial printing across different fabric types provides additional evidence that small-scale geometric modifications and substrate interactions can have disproportionate effects on tensile and flexural properties, reinforcing the need to study how circular pattern size and arrangement influence the performance of highly porous textiles like tulle [25–28].

These factors make tulle highly responsive to pattern-induced structural reinforcement, but also highly

vulnerable to pattern-induced stress concentrations. The porous mesh may allow substantial mechanical interlocking, but pattern rigidity can lead to premature rupture of the textile ligaments. The literature contains almost no systematic studies examining how 3D-printed patterns – especially circular patterns of varying size and spacing – affect the tensile behaviour of tulle. This represents a crucial knowledge gap, given the widespread use of tulle in fashion, costume design, scenography, and emerging fields requiring ultralight functional textiles.

Circular geometries are especially relevant because they distribute stresses uniformly, avoid sharp edges that typically concentrate stresses, lend themselves to parameterisation (diameter, spacing, arrangement), are aesthetically compatible with fashion and textile applications, and can act as isotropic reinforcement nodes in an anisotropic mesh fabric.

Patterns with varied circular sizes and arrangements provide a structured framework for investigating how discrete reinforcement zones modify the tensile properties of open-structured textiles. Such studies can lead to design guidelines applicable to both artistic and functional contexts, enabling the creation of robust, lightweight textile–polymer composites.

Mechanically, the printed circles can be conceptualised as localised rigid inclusions embedded within a compliant matrix (the tulle fabric). Under tensile loading, stress redistributes around these inclusions, with the degree of stress concentration being influenced by:

- circle diameter (larger elements stiffen greater surface area);
- spacing (tighter spacing increases composite stiffness);
- arrangement (grid, staggered, radial, alternating patterns);
- adhesion effectiveness (stronger bonding increases load transfer into polymer nodes);
- substrate anisotropy (tulle's warp/weft relation determines load paths).

Prior work on 3D-printed fabrics indicates that printed elements can either strengthen the substrate or induce premature failure depending on their rigidity relative to the textile [5, 16]. For tulle specifically, the interaction between polymer inclusions and mesh apertures likely plays a decisive role, suggesting a mixed-mode failure involving both textile rupture and interfacial detachment.

Given the scarcity of data on ultralight substrates in TAM research, the present study seeks to address a fundamental gap: How do circular 3D-printed patterns of different sizes and spatial arrangements influence the tensile properties of tulle fabric?

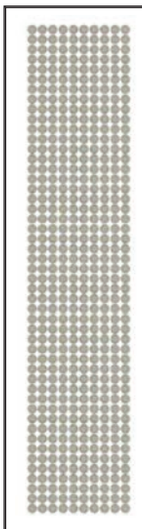
This work contributes to the field by providing the first systematic mechanical evaluation of 3D-printed circular patterns on tulle, comparing how diameter and arrangement affect strength/ stiffness/ elongation, examining interactions between polymer reinforcement nodes and delicate mesh structures, and generating design principles for future applications in lightweight hybrid textiles.

These insights have implications for industries seeking to integrate AM into fashion, performance costumes, millinery, wearable art, protective composites, and emerging metamaterial textiles.

MATERIALS AND METHODS

The primary material used in this research was tulle, a 100% polyester textile chosen for its fine mesh structure and lightweight properties. The tulle has a nominal thickness of approximately 0.23 mm and was supplied in the form of a swatch from which the test specimens were cut. Each tensile test specimen was a strip of tulle 50 mm wide and 250 mm long, of which 200 mm were effectively tested, with the remaining 50 mm clamped (in accordance with standard dimensions for tensile testing of textile strips). Various polymer models were 3D printed onto these tulle specimens using a 3D printer with Fused Deposition Modelling (FDM) additive manufacturing. The printing material was a polylactic acid (PLA) filament, chosen for its ease of printing, good adhesion to textile materials, and its sustainability as a biodegradable material. Before printing, each tulle sample was secured on the printer bed to keep it taut and stationary throughout the printing process.

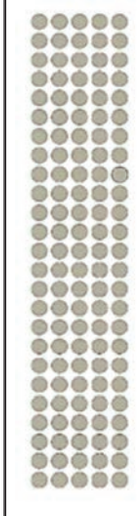
Four different geometrical patterns were designed using Autodesk Fusion software. The file was saved in *.stl format and later processed in Bambu Studio, where the printing operation was optimised by fitting 4 samples simultaneously. The print height was also adjusted to 6 layers (1 mm thickness). The printing parameters were modified, and the necessary pause was added between layers 1 and 2, at which point the textile substrate is added. The final step in obtaining the test samples involved slicing the files and printing the tulle specimens using the Bambu Lab P1P printer with PLA Basic filament from Bambu Lab, along with a control sample with no printing. The 3D printer was equipped with a 0.4 mm nozzle. A layer height of 0.16 mm was used for all printed structures, while the initial layer height was increased to 0.2 mm to enhance adhesion between the polymer and the textile substrate. The extrusion width was set to 0.42 mm to ensure dimensional accuracy and uniform deposition of the circular patterns. Printing speeds were adapted to ensure stable deposition on the flexible textile substrate. The initial layer speed was reduced to 50 mm/s to improve adhesion, while higher speeds were used for internal structures and infill (up to 200 mm/s) to optimise printing time. Acceleration parameters were set to 4000 mm/s² for standard printing and up to 10000 mm/s² for travel movements, ensuring efficient operation without inducing excessive mechanical stress on the textile. No support structures were required due to the planar geometry of the printed elements. A textured PEI build plate was used to ensure sufficient adhesion during printing without additional adhesives. The printing process was conducted in a layer-by-layer sequence, allowing partial penetration of the molten polymer into the tulle mesh, resulting in mechanical



SAC: **S**mall **A**ligned **C**ircles (50 x 10 pieces): A regular grid of small circular patches printed on the tulle. Each circle had a diameter of 4 mm, and circles were aligned in rows and columns (forming a straight lattice pattern along the warp and weft directions of the fabric). Adjacent circles in the grid were spaced with a centre-to-centre distance slightly larger than the diameter, such that the circles did not touch but were evenly distributed.

SSC: **S**mall **S**taggered **C**ircles (50 x 10 pieces): The same small circle diameter was used, but the pattern was arranged in an intercalated (staggered) manner. Rows of circles were offset such that each circle in a given row was positioned in the gap between circles in the adjacent rows (analogous to a hexagonal or triangular lattice arrangement). This staggered configuration spreads the circles more uniformly and avoids continuous straight columns of polymer.





LAC: **L**arge **A**ligned **C**ircles (25 x 5 pieces): A grid of larger circular patches (diameter 8 mm) printed in aligned rows/columns on the tulle. The spacing between these larger circles was set such that there were distinct gaps of bare fabric between patches, with circles aligned vertically and horizontally.

LSC: **L**arge **S**taggered **C**ircles (25 x 5 pieces): The same large circle size arranged in a staggered pattern (each row offset relative to the next), similar to the small staggered pattern but with larger features.



Fig. 1. The 3D-printed pattern geometries

interlocking at the interface. This mechanism has been identified as a key factor in improving adhesion between polymeric materials and textile substrates. The selected parameters were optimised to ensure a balance between adequate adhesion and the preservation of the textile structure. Lower initial layer speeds and increased first-layer thickness contributed to improved bonding, while controlled extrusion and acceleration parameters minimised deformation of the lightweight tulle fabric.

All patterns consisted of circular disk-shaped polymer patches, differing in size and arrangement, as presented in figure 1.

Each pattern was printed in 6 layers of filament approximately 1.1 mm thick, ensuring that the polymer just fused to the surface of the tulle without completely penetrating or excessively bulking the fabric. All printing was done with identical machine settings (nozzle diameter, layer height, print speed, and extrusion temperature) to maintain consistency; only the pattern geometry differed between samples. For each of the five sample types (one control and four patterned variants), multiple specimens (8 replicates per variant) were produced to ensure reproducibility of results (figure 2).

Because the experiment involves a textile and 3D-printed assembly, it can be treated analogously to a coating or applied layer. This makes it more justifiable than testing it as a purely textile sample (for which the original ISO 13934-1:2013 standard was designed), as the standard explicitly states that it is not usually applicable to coated fabrics [29].

For the present study, ISO 1421:2016 was considered one of the most relevant standards: 'Rubber- or plastics-coated fabrics – Determination of tensile strength and elongation at break' [30]. This standard covers fabrics coated with plastics or rubber and is therefore more closely aligned with the present research scenario of 'fabric + 3D printed layer'.

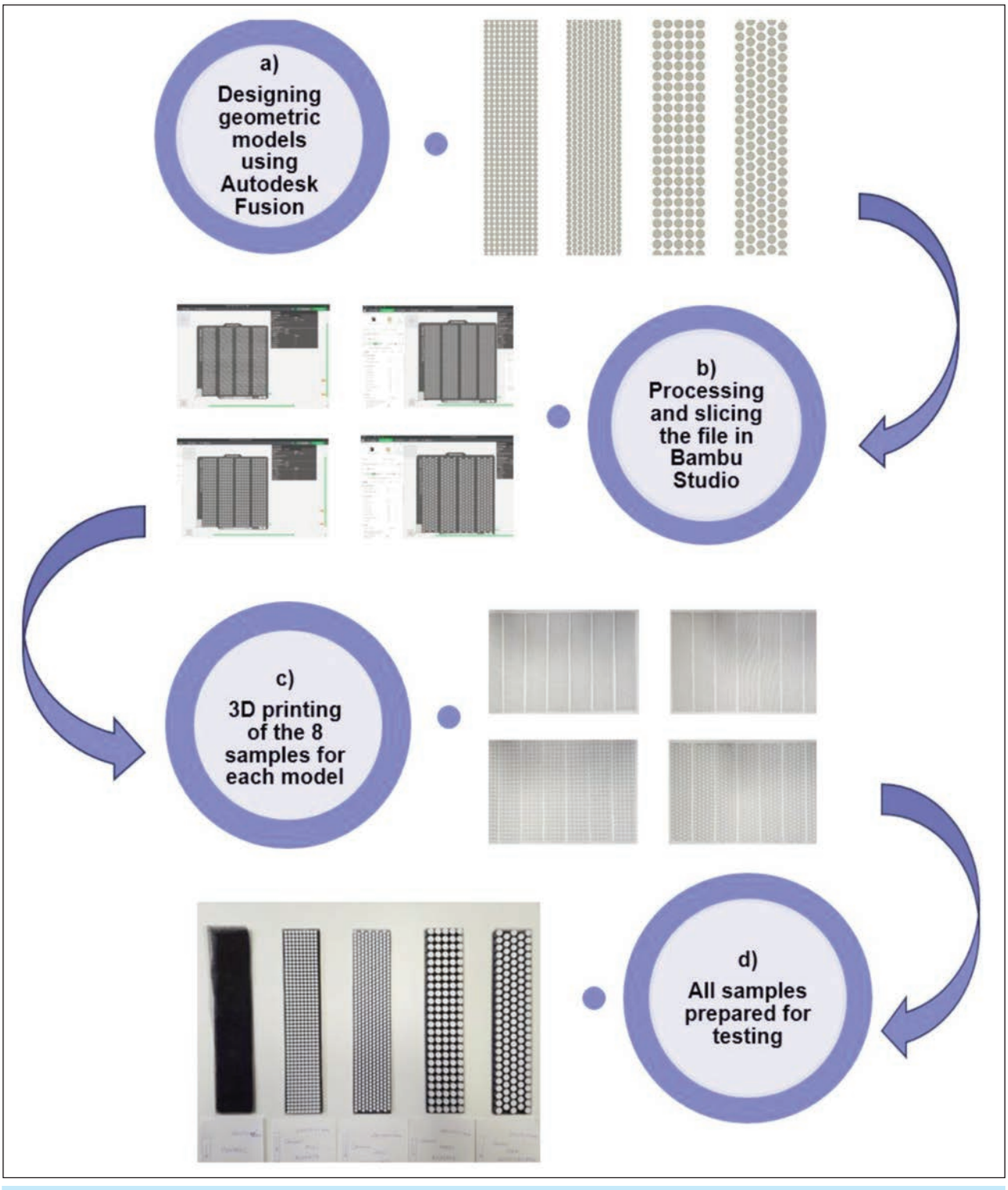


Fig. 2. The stages of making test samples

As such, ISO 1421:2016 was adopted as the methodological basis, with some adaptations, since the most important requirement for conducting a comparative test between unprinted tulle specimens and 3D printed tulle specimens, beyond complying with standard procedures, is to ensure that all samples are tested under identical conditions, including:

- specimen geometry (same width and same gauge length);
- testing machine and settings (same tensile speed, same type and size of grips);
- environmental conditions (same temperature and humidity);
- parameter definitions (% elongation, breaking strength in N/mm, maximum force in N, Young's modulus in N/mm²).

To ensure comparability, the "strip" method from ISO 1421 was used, applying the following test parameters:

- specimen width: 50 mm;
- specimen length: 200 mm;
- test speed: 100 mm/min.



Fig. 3. Testing the samples at STM 466

After printing, all samples were conditioned under standard laboratory atmosphere (approximately 20 ± 2°C and 65% ± 5 relative humidity) and stored in zipper bags with desiccant for at least 24 hours before testing, to minimise any influence of temperature or moisture on the behaviour of the fabric or polymer. Uniaxial tensile tests were performed using a universal testing machine ("Tensile Testing Centre STM 466"). Each specimen was clamped with an initial gauge length (distance between grips) of 200 mm. Tensile load was applied at a constant crosshead speed of 100 mm/min until the specimen failed. During each test, force–extension data were continuously recorded. The main mechanical parameters were derived from the force–extension curves: maximum force at break (peak load, which for a given sample width corresponds to tensile strength), elongation at break (extension at the breaking point, expressed as a percentage of the initial gauge length), and initial elastic stiffness (quantified by Young's modulus or initial slope, calculated within the linear elastic region of the curve).

The testing procedure was identical for all sample types. For printed specimens, care was taken to ensure that the orientation of the printed pattern relative to the loading direction was consistent: aligned patterns had rows of circles oriented either parallel or perpendicular to the loading direction (warp/weft alignment). In contrast, for staggered patterns, the grid's general axis of symmetry was aligned with the loading direction. After testing, the fracture surfaces of selected specimens were visually examined to qualitatively assess failure modes (e.g., yarn breakage in the tulle, print detachment, or a combination of both).

All measured data were collected and averaged for each sample group, and results were compared to evaluate the effect of pattern geometry on tensile performance (figure 3).

RESULTS AND DISCUSSION

The data reveal distinct mechanical behaviour of the tulle fabric depending on the geometry of the 3D-printed pattern applied to its surface and the testing direction (warp direction – column-wise vs. weft direction – row-wise).

The unprinted specimens (Control) exhibited the highest values for Young's modulus and elongation, indicating a homogeneous, elastic, and strong textile network. Overall, 3D printing reduced stiffness and elasticity, though in some cases it increased maximum force and breaking strength. The warp direction (columns) consistently demonstrated greater stiffness and strength than the weft direction (rows), regardless of the printed pattern geometry (tables 1 and 2).

Elongation at break (%)

The control sample, unprinted tulle, exhibited very high elasticity in the row (weft) direction, with an average elongation of 85.11%, which is typical for a thin textile material with a wide-mesh structure.

After 3D printing, the elongation was significantly reduced:

- 0 – Control sample: 85.11%
- SAC (small aligned circles): 33.86%
- SSC (small staggered circles): 37.93%
- LAC (large aligned circles): 28.79%
- LSC (large staggered circles): 29.04%

In the column (warp) direction, where extensibility is naturally lower, the values were even more reduced:

- 0 – Control sample: 26.76%
- SAC: 20.66%
- SSC: 18.22%
- LAC: 14.67%
- LSC: 14.61%.

It can be observed that 3D printing limits the deformability of the textile fibres, with the large circle patterns (LAC, LSC) being the most rigid and thus the least extensible in both directions (figure 4).

Table 1

THE AVERAGE VALUES MEASURED FOR THE COLUMN TESTING DIRECTION AND FOR DIFFERENT SAMPLES								
Control sample, 0 – unprinted tulle (column direction)								
0	Elongation (%)	Area (mm^2)	Breaking strength (N/mm)	Maximum force (N)	Sample length (mm)	Sample width (mm)	Thickness (mm)	Young's modulus (N/mm^2)
Mean	26.761	11.500	5.345	267.229	200.000	50.000	0.230	1412.654
Std Dev	2.210	0.000	0.708	35.421	0.000	0.000	0.000	47.318
Max	30.610	11.500	6.552	327.600	200.000	50.000	0.230	1469.699
Min	23.410	11.500	4.530	226.500	200.000	50.000	0.230	1347.766
3D-printed tulle sample with small aligned circles, SAC (column direction)								
SAC	Elongation (%)	Area (mm^2)	Breaking strength (N/mm)	Maximum force (N)	Sample length (mm)	Sample width (mm)	Thickness (mm)	Young's modulus (N/mm^2)
Mean	20.656	11.500	6.566	328.300	200.000	50.000	1.100	285.031
Std Dev	0.663	0.000	0.212	10.612	0.000	0.000	0.000	12.498
Max	21.163	11.500	6.780	339.000	200.000	50.000	1.100	305.956
Min	19.425	11.500	6.254	312.700	200.000	50.000	1.100	273.203
3D-printed tulle sample with small staggered circles, SSC (column direction)								
SSC	Elongation (%)	Area (mm^2)	Breaking strength (N/mm)	Maximum force (N)	Sample length (mm)	Sample width (mm)	Thickness (mm)	Young's modulus (N/mm^2)
Mean	18.221	11.500	6.281	314.300	200.000	50.000	1.100	309.298
Std Dev	1.649	0.000	0.629	31.748	0.000	0.000	0.000	12.831
Max	20.838	11.500	7.126	358.200	200.000	50.000	1.100	321.423
Min	15.500	11.500	5.204	260.500	200.000	50.000	1.100	283.221
3D-printed tulle sample with large aligned circles, LAC (column direction)								
LAC	Elongation (%)	Area (mm^2)	Breaking strength (N/mm)	Maximum force (N)	Sample length (mm)	Sample width (mm)	Thickness (mm)	Young's modulus (N/mm^2)
Mean	14.672	11,500	6.205	312.143	200.000	50.000	1.100	418.911
Std Dev	0.935	0.000	0.349	19.718	0.000	0.000	0.000	32.669
Max	15.713	11.500	6.718	336.700	200.000	50.000	1.100	469.050
Min	12.925	11.500	5.698	284.900	200.000	50.000	1.100	385.790
3D-printed tulle sample with large staggered circles, LSC (column direction)								
LSC	Elongation (%)	Area (mm^2)	Breaking strength (N/mm)	Maximum force (N)	Sample length (mm)	Sample width (mm)	Thickness (mm)	Young's modulus (N/mm^2)
Mean	14.611	11.500	6.162	310.763	200.000	50.000	1.100	410.402
Std Dev	1.228	0.000	0.449	20.651	0.000	0.000	0.000	7.052
Max	16.800	11.500	6.954	347.700	200.000	50.000	1.100	418.591
Min	13.475	11.500	5.776	297.000	200.000	50.000	1.100	394.968

Table 2

THE AVERAGE VALUES MEASURED FOR THE ROW TESTING DIRECTION AND FOR DIFFERENT SAMPLES								
Control sample, 0 – unprinted tulle (row direction)								
0	Elongation (%)	Area (mm^2)	Breaking strength (N/mm)	Maximum force (N)	Sample length (mm)	Sample width (mm)	Thickness (mm)	Young's modulus (N/mm^2)
Mean	85.1105	11.500	1.279	101.588	200.000	50.000	0.230	128.337
Std Dev	8.567	0.000	0.835	12.935	0.000	0.000	0.000	5.806
Max	94.620	11.500	2.400	123.200	200.000	50.000	0.230	140.230
Min	69.400	11.500	0.314	79.300	200.000	50.000	0.230	121.023

THE AVERAGE VALUES MEASURED FOR THE ROW TESTING DIRECTION AND FOR DIFFERENT SAMPLES								
3D-printed tulle sample with small aligned circles, SAC (row direction)								
SAC	Elongation (%)	Area (mm^2)	Breaking strength (N/mm)	Maximum force (N)	Sample length (mm)	Sample width (mm)	Thickness (mm)	Young's modulus (N/mm^2)
Mean	33.859	11.500	1.439	105.483	200.000	50.000	1.100	73.378
Std Dev	4.143	0.000	0.885	1.973	0.000	0.000	0.000	2.481
Max	39.888	11.500	2.032	108.300	200.000	50.000	1.100	75.711
Min	28.638	11.500	0.212	102.400	200.000	50.000	1.100	69.674
3D-printed tulle sample with small staggered circles, SSC (row direction)								
SSC	Elongation (%)	Area (mm^2)	Breaking strength (N/mm)	Maximum force (N)	Sample length (mm)	Sample width (mm)	Thickness (mm)	Young's modulus (N/mm^2)
Mean	37.930	11.500	1.717	104.313	200.000	50.000	1.100	70.656
Std Dev	3.025	0.000	0.391	1.835	0.000	0.000	0.000	3.286
Max	42.263	11.500	1.986	106.700	200.000	50.000	1.100	75.057
Min	32.988	11.500	0.918	102.000	200.000	50.000	1.100	65.957
3D-printed tulle sample with large aligned circles, LAC (row direction)								
LAC	Elongation (%)	Area (mm^2)	Breaking strength (N/mm)	Maximum force (N)	Sample length (mm)	Sample width (mm)	Thickness (mm)	Young's modulus (N/mm^2)
Mean	28.791	11.500	0.938	98.575	200.000	50.000	1.100	89.780
Std Dev	4.560	0.000	0.808	2.366	0.000	0.000	0.000	6.450
Max	34.888	11.500	1.962	101.600	200.000	50.000	1.100	97.693
Min	23.488	11.500	0.172	94.200	200.000	50.000	1.100	83.431
3D-printed tulle sample with large staggered circles, LSC (row direction)								
LSC	Elongation (%)	Area (mm^2)	Breaking strength (N/mm)	Maximum force (N)	Sample length (mm)	Sample width (mm)	Thickness (mm)	Young's modulus (N/mm^2)
Mean	29.038	11.500	0.538	91.238	200.000	50.000	1.100	98.373
Std Dev	2.970	0.000	0.479	2.730	0.000	0.000	0.000	2.202
Max	34.525	11.500	1.554	96.100	200.000	50.000	1.100	100.728
Min	24.750	11.500	0.156	88.300	200.000	50.000	1.100	95.118

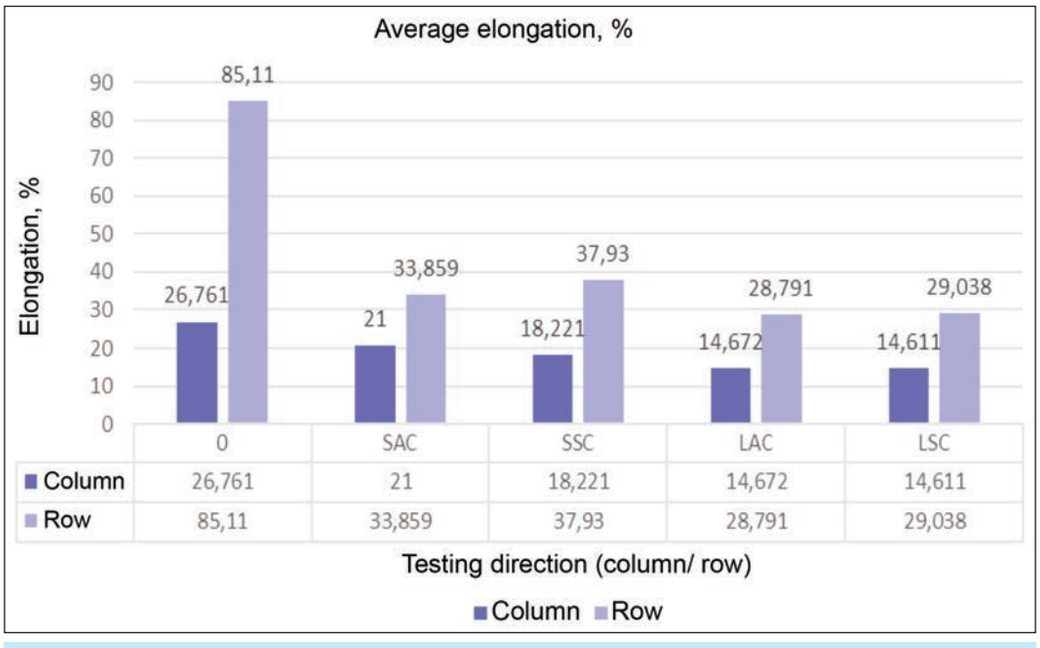


Fig. 4. Average elongation (%) depending on the testing direction

Breaking strength (N/mm)

An interesting observation is that the breaking strength increased in the column (warp) direction for all the printed samples:

- 0 – Control sample: 5.345 N/mm
- SAC (small aligned circles): 6.566 N/mm
- SSC (small staggered circles): 6.281 N/mm
- LAC (large aligned circles): 6.205 N/mm
- LSC (large staggered circles): 6.162 N/mm.

This suggests that the printed material absorbs part of the mechanical load, delaying complete rupture.

In the row (weft) direction, the values are significantly lower, but a strengthening effect is observed for:

- SSC: 1.717 N/mm (compared to 1.279 N/mm in the control)
- SAC: 1.439 N/mm.

The large circle patterns (LAC, LSC) performed poorly in this direction, likely due to stress concentration at the edges of the printed zones. Overall, 3D printing brings structural benefits in the warp direction, but it may cause local weakening in the transverse direction depending on the printed geometry (figure 5).

Maximum force (N)

The maximum force follows a similar trend to the breaking strength, but it reflects the overall load-bearing capacity rather than just the point of break.

In the column (warp) direction, all printed models outperformed the control sample:

- 0 – Control sample: 267.229 N
- SAC (small aligned circles): 328.300 N (highest value)
- SSC (small staggered circles): 314.300 N
- LAC (large aligned circles): 312.143 N
- LSC (large staggered circles): 310.763 N.

In the row (weft) direction, although the values are lower overall, all printed models recorded comparable or higher forces than the control:

- 0 – Control sample: 101.588 N
- SAC: 105.483 N
- SSC: 104.313 N.

The printed layer acts as a reinforcement within the mechanical structure of the sample. Even with reduced elongation, the total force sustained by the material increases significantly, especially in the warp direction (figure 6).

Young's modulus (N/mm²)

In the column (warp) direction, the control sample (unprinted tulle) exhibited a high average Young's modulus of 1412.65 N/mm², indicating a rigid and low-extensibility structure. In contrast, all four printed models showed a substantial decrease:

- SAC (small aligned circles): 285.03 N/mm²
- SSC (small staggered circles): 309.30 N/mm²
- LAC (large aligned circles): 418.91 N/mm²
- LSC (large staggered circles): 410.40 N/mm².

The significant drop in stiffness suggests that the addition of the printed material alters the stress distribution within the tulle's mesh structure.

In the row (weft) direction, where tulle is naturally more flexible, the Young's modulus was lower even in the control sample (128.34 N/mm²). The printed patterns resulted in a slight increase in stiffness, particularly for:

- LSC: 98.37 N/mm²
- LAC: 89.78 N/mm².

The denser coverage and geometry of the printed material (in the LSC and LAC models) provide additional resistance in the weft direction. However, it does not reach the inherent stiffness levels observed in the warp direction (figure 7).

Qualitative analysis of the failure

Following the tensile tests, it was observed that most specimens ruptured near the edge of the grip jaws, at

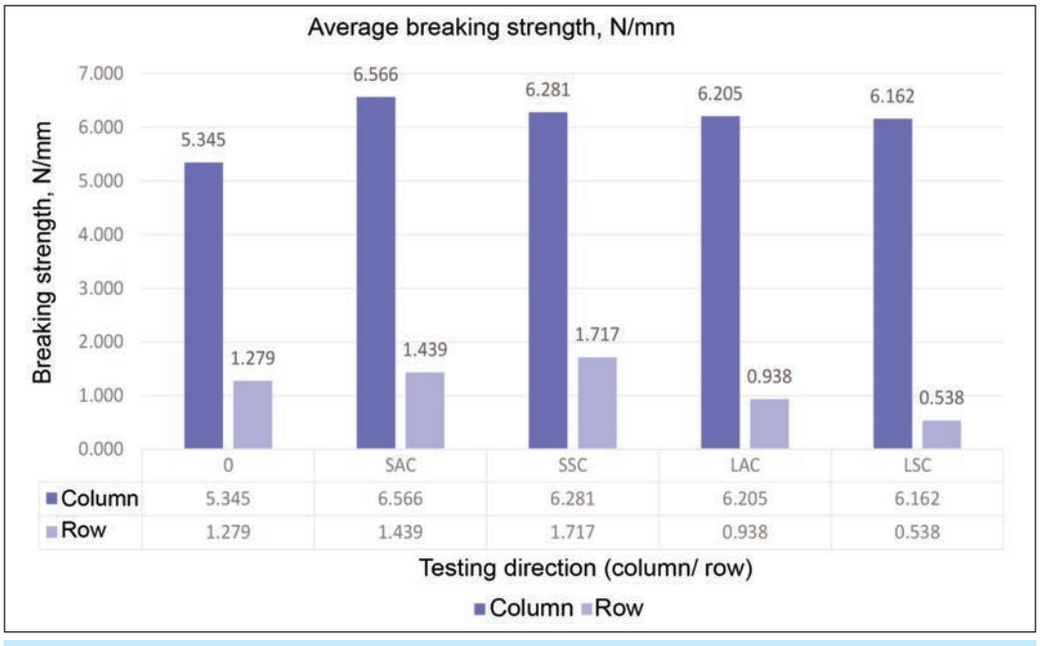


Fig. 5. Average breaking strength (N/mm) depending on the testing direction

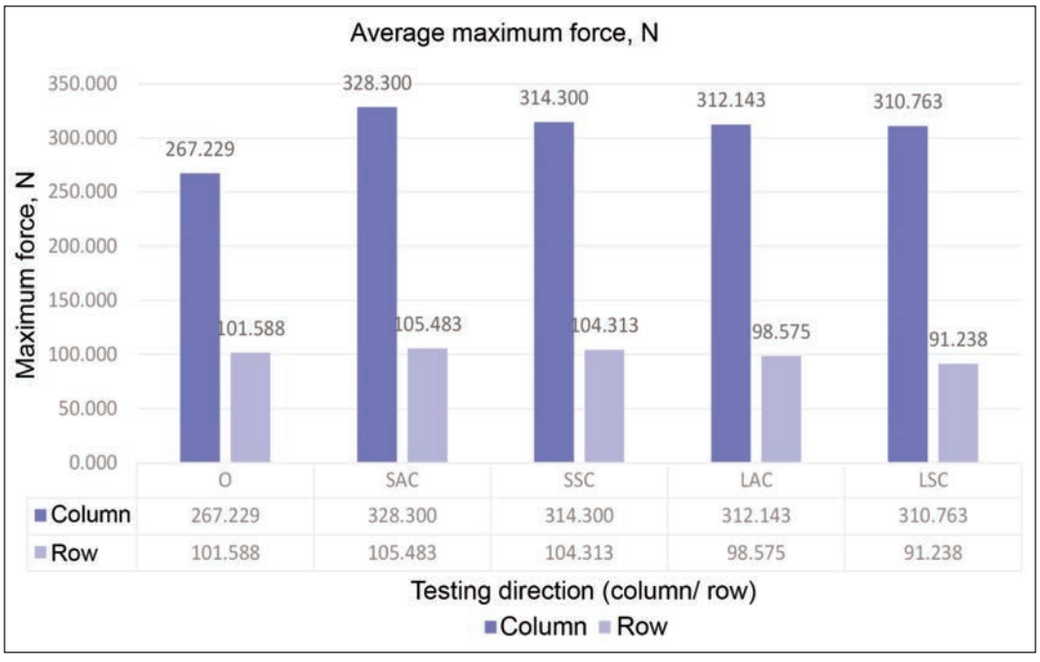


Fig. 6. Average Maximum force (N) depending on the testing direction

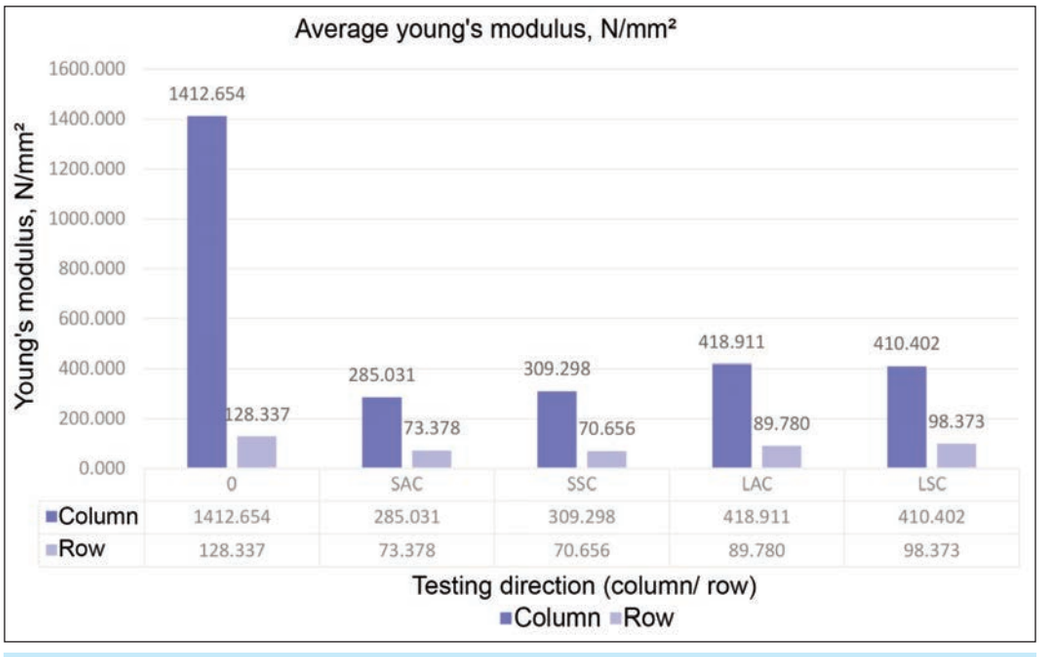


Fig. 7. Average Young's modulus (N/mm^2) depending on the testing direction

the boundary between the clamped and free portions of the sample. According to ISO 1421, the rupture should occur in the central region between the clamps, so that the stress distribution accurately reflects the material's mechanical behaviour.

However, considering the specific nature of the tested material, tulle, a lightweight, perforated, and flexible textile, the rupture at the jaw boundary can be explained by:

- stress concentration within the mesh openings in contact with the grip surface;
- local deformation of the material due to mechanical clamping pressure;
- the atypical behaviour of net-like materials, which do not allow for uniform stress distribution.

To limit this effect, appropriate gripping accessories were used, and the tests were conducted with careful specimen alignment. Since all samples were subjected to the same testing protocol and exhibited consistent rupture behaviour, the results were considered valid and relevant for comparing the printed and unprinted tulle variants.

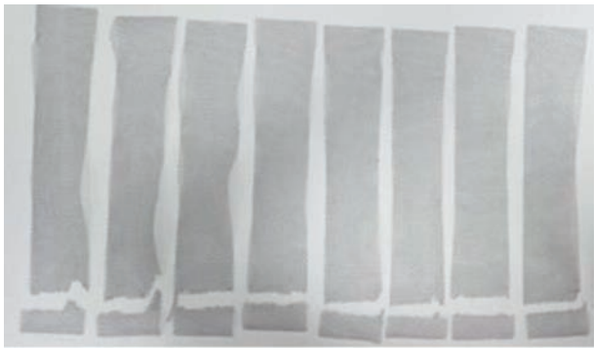
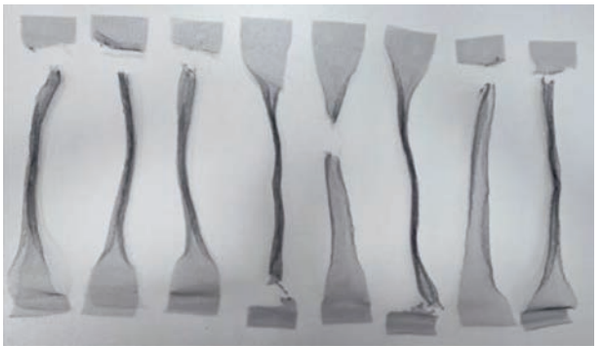
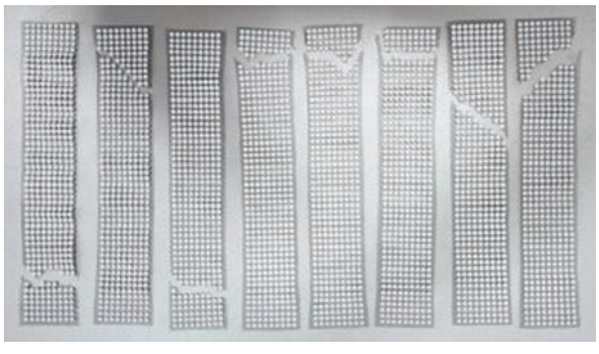
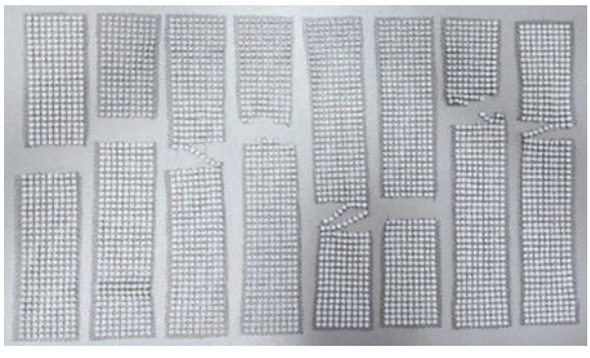
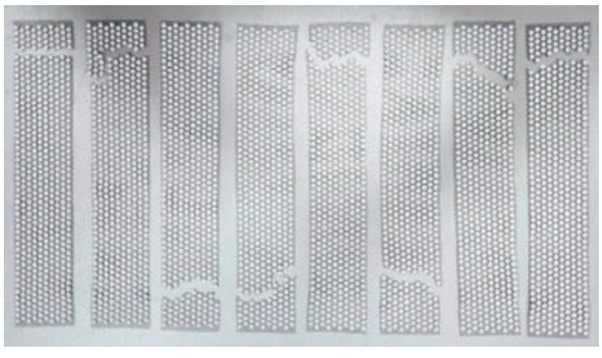
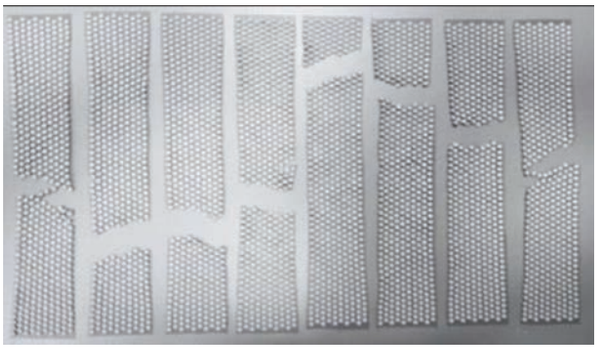
Table 3 presents the qualitative visual appearance of the samples after uniaxial tensile testing and an analysis of post-tested samples by direction, organised as follows:

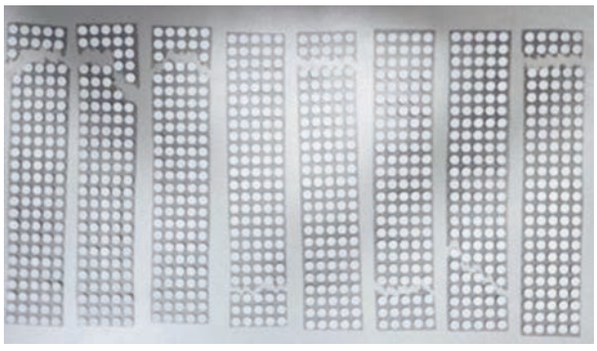
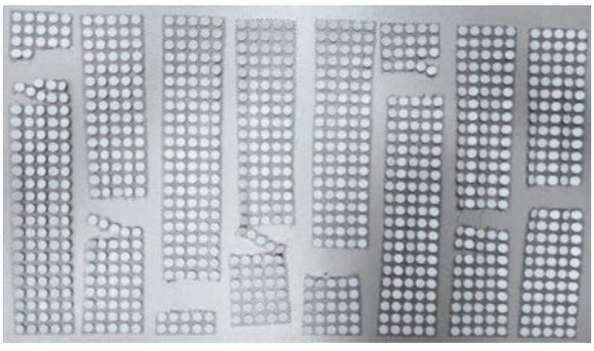
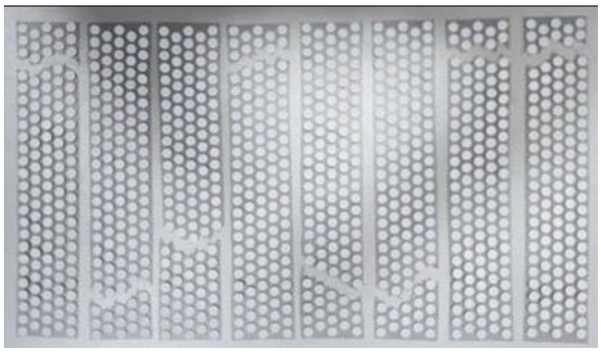
- Left column: samples tested in the column/warp direction;
- Right column: samples tested in the row/weft direction.

Each row corresponds to a different sample type (from unprinted tulle to various 3D-printed geometries). Distinct fracture patterns are evident, influenced by the load orientation and print configuration.

Table 3

QUALITATIVE ANALYSIS OF THE FAILURE MODE OF THE SAMPLES

Column (left)	**Row (right)**
	
0 – Control samples (unprinted tulle)	
Column direction: Clean, abrupt tears occur just outside the jaw grips, highlighting stress concentration at the clamp exit. The homogeneous textile mesh allows a uniform strain response.	**Row direction (right)**: Significant necking and elongation are visible before rupture, typical of the more elastic weft orientation. The mesh stretches significantly, often leading to irregular edge curling.
	
SAC – Small Aligned Circles	
Column direction: Fracture paths follow vertical lines, occasionally crossing through the printed rows. The alignment seems to channel stress along narrow paths, increasing fracture predictability but also brittleness.	**Row direction**: The breaks are more chaotic, frequently passing diagonally through the printed areas. Misalignment between circles and load direction may have created zones of uneven rigidity and localised failure.
	
SSC – Small Staggered Circles	
Column direction: Cracks appear fragmented and irregular, often bypassing dense print areas. The staggered configuration appears to better diffuse mechanical stress, leading to distributed rather than concentrated rupture.	**Row direction**: Jagged tears cut across the interspersed print pattern, and multiple samples show complex, branching failure lines. This suggests higher ductility or delayed intention to failure in the weft direction for this pattern.

QUALITATIVE ANALYSIS OF THE FAILURE MODE OF THE SAMPLES	
	
LAC – Large Aligned Circles	
Column direction: Several breaks occur through or around large circles, with clear stress risers near the printed edges. In some samples, minor delamination between PLA and tulle fabric is visible.	**Row direction**: Breakage often propagates between adjacent rows of circles, especially at lower printing density. The directionality of the aligned print may have acted like fault lines under stress.
	
LSC – Large Staggered Circles	
Column direction: Breaks follow less predictable paths than LAC. The staggered layout appears to distribute stress more evenly, but it still leaves weak points in overlapping zones.	**Row direction**: Tearing occurs in dispersed zones across the mesh. In some samples, the failure does not cut directly through the centre but follows less obvious load paths, likely due to the interaction between mesh and print.

In conclusion, it can be said that column direction testing (left) consistently yields straighter, more defined fracture lines, emphasising the natural stiffness and limited extensibility of the warp threads, whilst the row direction testing (right) results in more variable and complex break patterns, highlighting the deformability of the weft and how print geometries interact with a more compliant base. Denser, more regular geometries (e.g., aligned circles) tend to promote brittle, concentrated fractures, whereas staggered, less constrained layouts delay failure and encourage more distributed rupture behaviour. Visual evidence of partial PLA delamination or localised detachment was occasionally observed in more rigid geometries, especially LAC and LSC.

Analysis of stress-strain curves

As the graphs illustrate, for the 0 – Control Samples (Column/Warp Direction), the curves exhibit a steep initial slope, indicating high stiffness and low initial deformation, characteristic of warp threads which are more tightly tensioned during weaving. In the linear elastic region, most curves exhibit a linear rise at the beginning, typical of elastic behaviour before yield. Maximum load (peak force) is significantly higher in this direction, consistent with the numerical data (e.g., ~270 N). A sharp drop after the peak is evident, and a sudden rupture is observed, suggesting brittle-like failure in the warp direction. The curves are consistent across samples, indicating high repeatability and uniform mechanical behaviour of the unprinted tulle in this direction. Regarding the failure mode, the graph suggests that failure occurs when the material reaches its maximum load-bearing capacity, accompanied by minor plastic deformation.

For the 0 – Control Samples (Row/Weft Direction), these curves are generally more gradual, with shallower slopes, reflecting higher extensibility and lower stiffness than in the warp direction (figure 8). The samples exhibit greater extension before rupture; they stretch farther before failure, which is consistent with the elongation data (e.g., ~85% strain). The graph shows lower peak forces; the maximum load is significantly lower (~100 N), which aligns with the

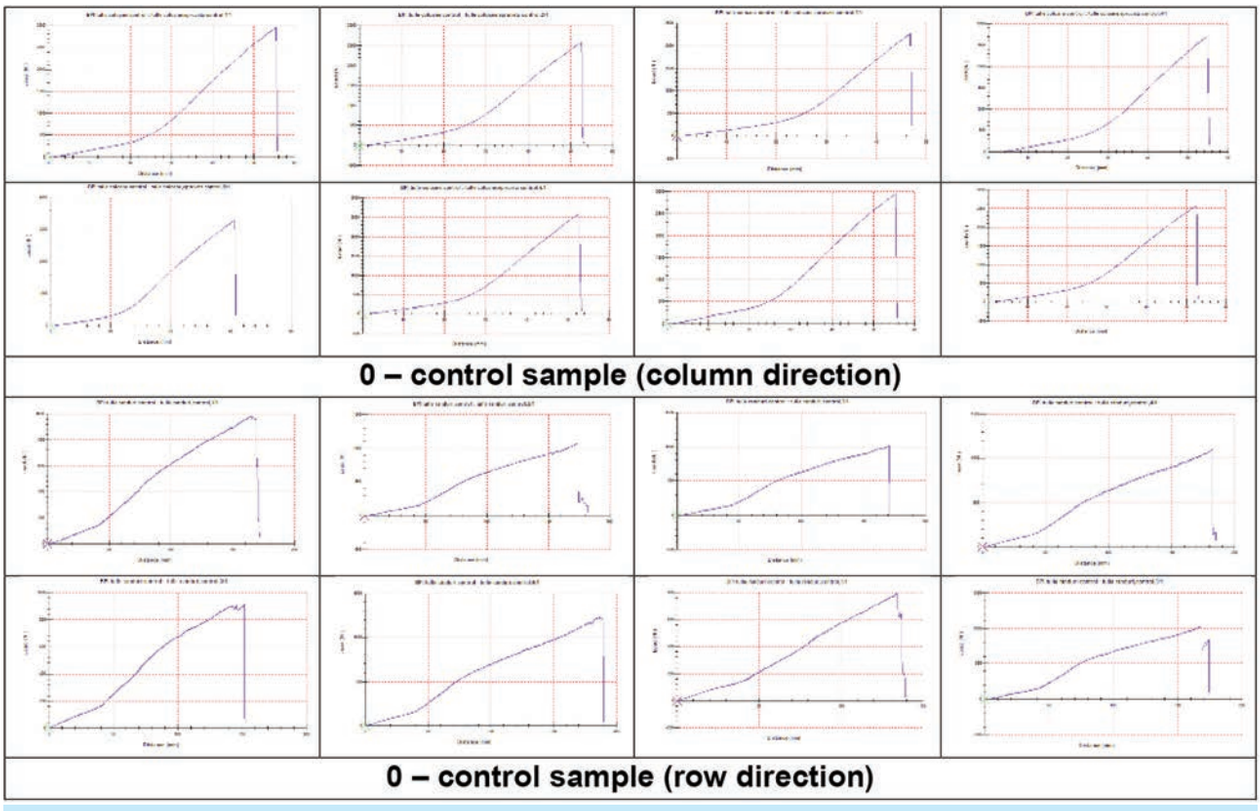


Fig. 8. The load-distance (force-extension) graphs for the 0 – Control samples (column/ row direction)

weft's structural properties (less-dense yarns, more open mesh). Some curves exhibit nonlinear behaviour early in the test, likely due to gradual thread engagement or mesh deformation. The post-yield region is more visible in some samples, with a plateau or slow increase before rupture, suggesting more ductile behaviour. Small fluctuations in the curves before failure (zigzag or dips) might be due to mesh deformation, thread slipping or reorientation before total rupture.

Overall, the unprinted tulle material behaves differently in each principal direction due to the anisotropic nature of woven fabrics. In the warp (column) direction, the structure is stronger and stiffer, bearing more load but failing more abruptly. In the weft (row) direction, the material is more deformable, stretching considerably before failure but unable to withstand high forces. These baseline behaviours help evaluate the reinforcement or degradation introduced by the 3D-printed patterns in later sample sets.

The curves for the SAC – Small Aligned Circles (Column Direction) are moderately steep, with a noticeable elastic region followed by a distinct peak, similar to the control column samples but with lower slopes, indicating reduced stiffness (figure 9). The maximum force is generally higher than the control, confirming the reinforcing effect of the 3D-printed pattern along the column (warp) direction. All samples demonstrate abrupt drops after the peak, characteristic of brittle-like rupture, despite the added 3D material. Compared to the control, the curves show slightly more gradual rises, indicating some loss in rigidity, but overall stronger peak values, consistent with previously reported average maximum forces (~328 N). The small, 3D-printed aligned circles act as load-bearing elements, transferring stress across the tulle and enhancing its resistance to force until rupture. The consistent peak and rupture across samples imply good repeatability and suggest the aligned pattern works well in the warp direction.

The curve for SAC – Small Aligned Circles (Row Direction) shows a more gradual slope and fewer sharp peaks, indicating lower stiffness and more ductile behaviour than in the column direction. There is a notable variation in post-peak behaviour; some curves drop sharply, while others show jagged, irregular fluctuations, possibly indicating progressive local failure, filament delamination, or cracking in the print. Despite lower stiffness, maximum forces are slightly higher than those of the unprinted control (e.g., ~105 N vs. 101 N), consistent with earlier quantitative results. Overall, the SAC pattern improves load-bearing capacity but also introduces heterogeneous stress concentrations, especially where the alignment doesn't align with the load path. The non-smooth post-peak behaviour suggests complex failure modes, likely a combination of tulle thread breakage and partial delamination or failure of the printed PLA.

The SAC geometry performs best in the column direction, where its alignment reinforces the warp threads. In the row direction, while there is some mechanical benefit, the alignment of small circles does not follow the primary strain path, leading to less efficient reinforcement and more complex failure behaviour. Overall, this pattern offers a balanced

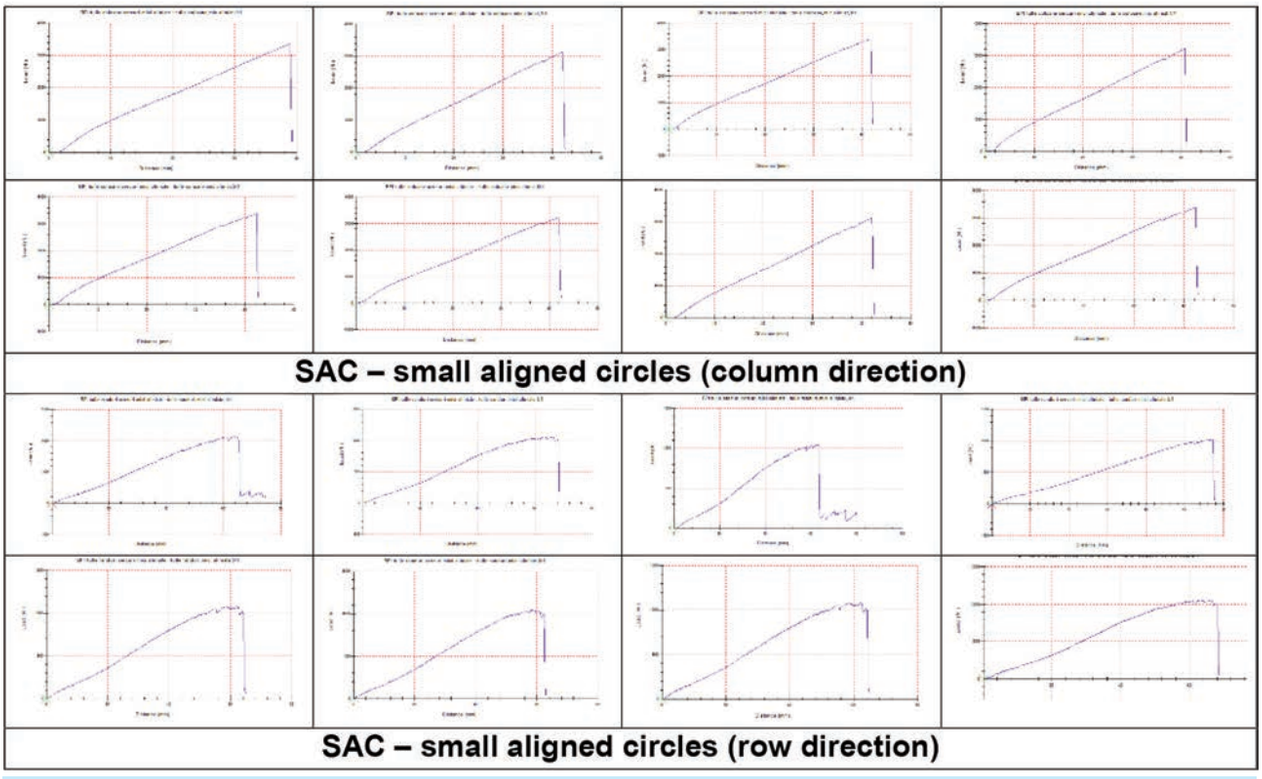


Fig. 9. The load-distance (force-extension) graphs for the SAC – Small Aligned Circles samples (column/ row direction)

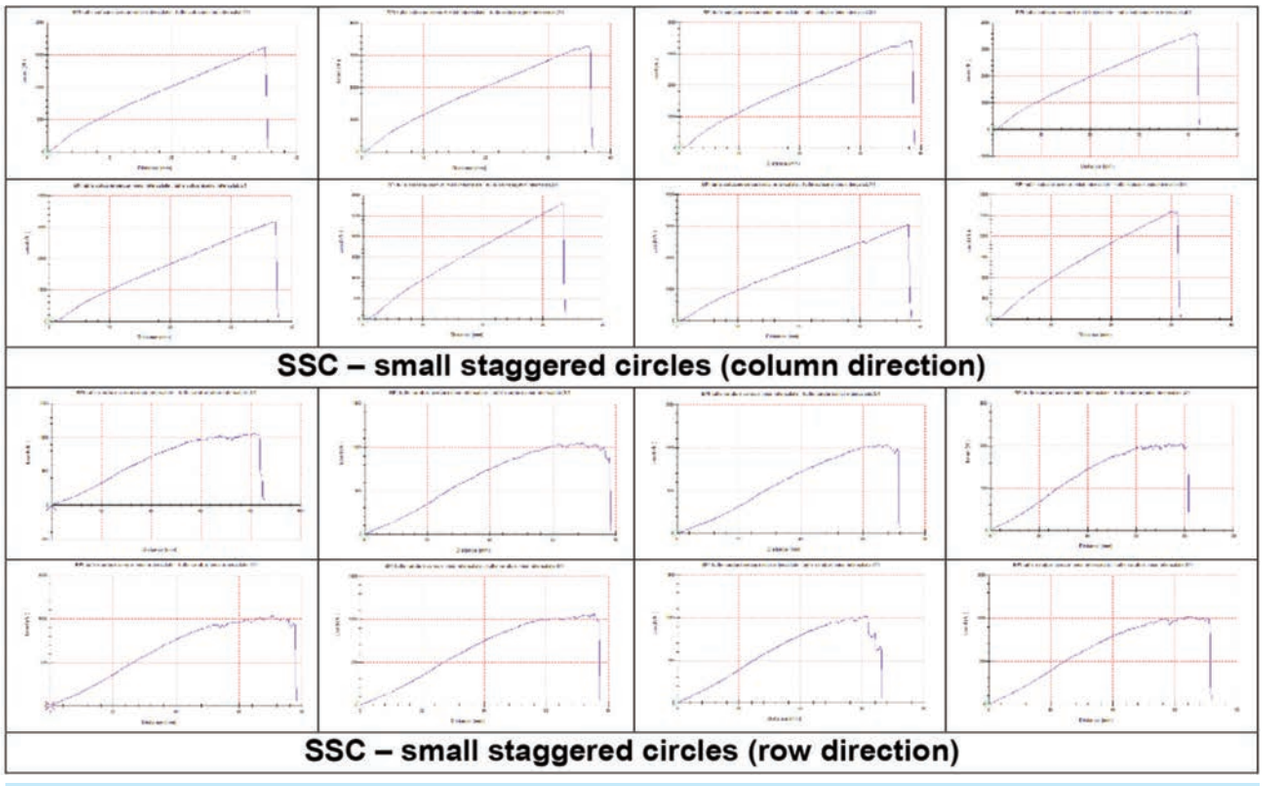


Fig. 10. The load-distance (force-extension) graphs for the SSC – Small Staggered Circles samples (column/row direction)

trade-off between reinforcement and flexibility, with better results when aligned with the principal load direction.

For the SSC – Small Staggered Circles (column direction), the force–extension curves for this geometry are consistent and highly repeatable, with linear increases followed by abrupt drops, indicating clear fracture points (figure 10). The slopes are similar to those observed in SAC (aligned circles), but slightly steeper in some cases, suggesting greater stiffness in the intercalated geometry. The maximum load appears comparable to or somewhat lower than

SAC, but remains higher than the control, confirming that the printed pattern strengthens the structure in the warp direction. Rupture occurs suddenly and consistently across all samples, which reflects uniform material response. The staggered arrangement of small circles contributes to homogeneous stress distribution, reducing the chance of premature failure along single filament lines. Compared to SAC, SSC might better distribute forces laterally, explaining slightly more consistent slopes and rupture points. The structure reinforces without excessively compromising deformability, which is favourable in high-load warp-oriented applications.

The curve behaviour for the SSC – Small Staggered Circles (row direction) shows greater elongation before failure and more complex post-peak behaviour, including plateaus, jagged declines, and progressive drops. The force–distance curves are flatter, indicating lower stiffness in the column direction. Several samples exhibit non-linear, gradual failures, likely reflecting a ductile-like progression, with staggered geometry delaying complete rupture. Compared to the SAC row curves, SSC exhibits slightly smoother transitions and possibly better energy absorption, as indicated by a wider curve. The staggered layout improves load redistribution, reducing the likelihood of abrupt failures. The gradual loss of load-bearing capacity post-peak suggests delamination or cracking of the PLA pattern before rupture of the tulle thread. While overall force values are still lower than those in the column direction, SSC performs relatively better than SAC in the row direction, likely due to the offset pattern reinforcing more cross-threads.

In the column direction, SSC samples demonstrate reliable mechanical strength with consistent performance, reinforcing the idea that intercalated geometries enhance structural continuity. In the row direction, the geometry enables controlled failure and better deformation tolerance, providing superior ductility and resilience compared to SAC. Overall, SSC represents a balanced configuration that enhances both strength and flexibility depending on load orientation, making it suitable for applications requiring durability and controlled deformation.

The load–distance graphs for the LAC – Large Aligned Circles (column direction) show a linear-elastic region followed by a clear peak and a sudden drop, consistent with brittle-type rupture (figure 11). Compared to SAC and SSC, the curves here tend to have slightly lower slopes, suggesting a moderate reduction in stiffness. Maximum loads are high and quite consistent, with very little dispersion among samples, indicating that the large aligned circles provide strong structural support in the warp direction. Rupture occurs abruptly, indicating uniform stress build-up followed by rapid failure, likely along the printed ring outlines. The large aligned circles act as rigid printed zones that transfer and concentrate loads, allowing the sample to resist significant force until a critical failure point is reached. While this improves maximum force capacity, it may compromise ductility, as seen in the sudden, sharp rupture profiles. This geometry is effective at strengthening tulle in the warp/column direction, though with reduced elasticity.

For the LAC – Large Aligned Circles (row direction), these graphs are more irregular, with plateau-like

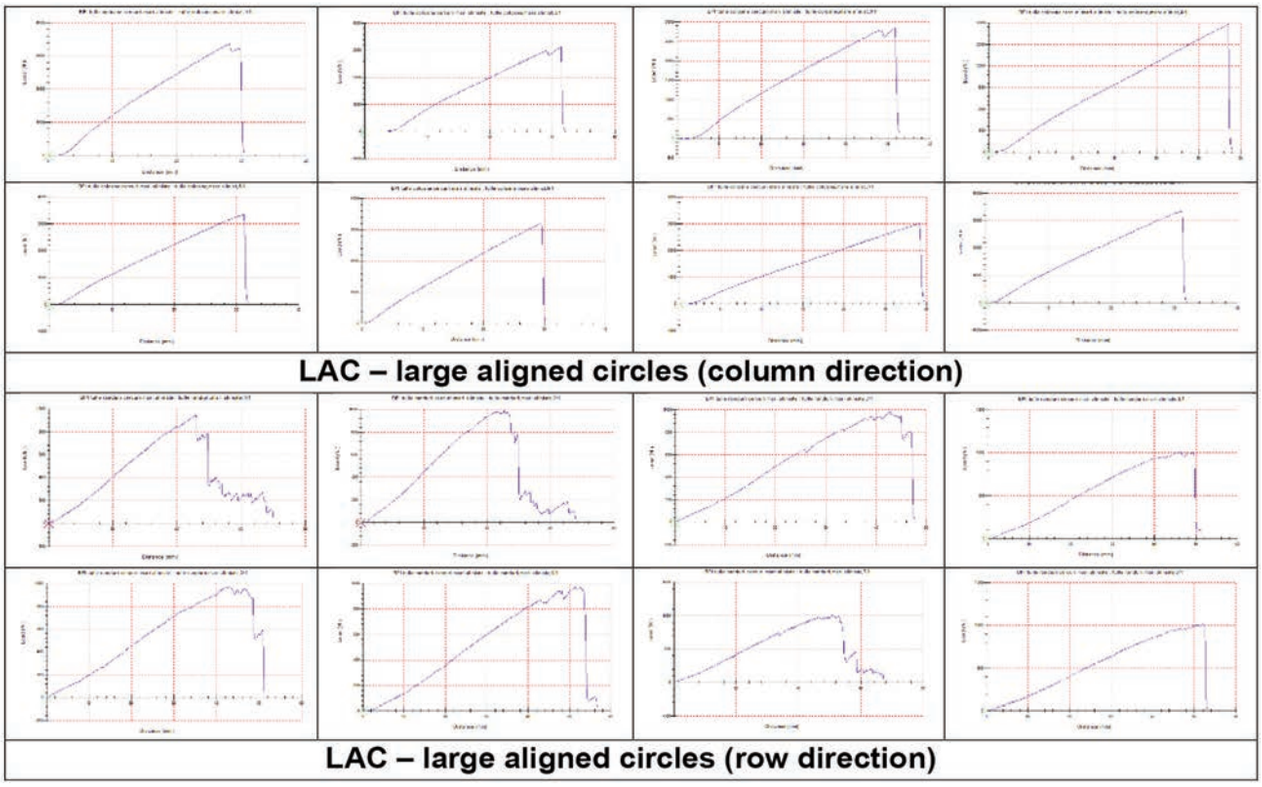


Fig. 11. The load-distance (force-extension) graphs for the LAC – Large Aligned Circles samples (column/ row direction)

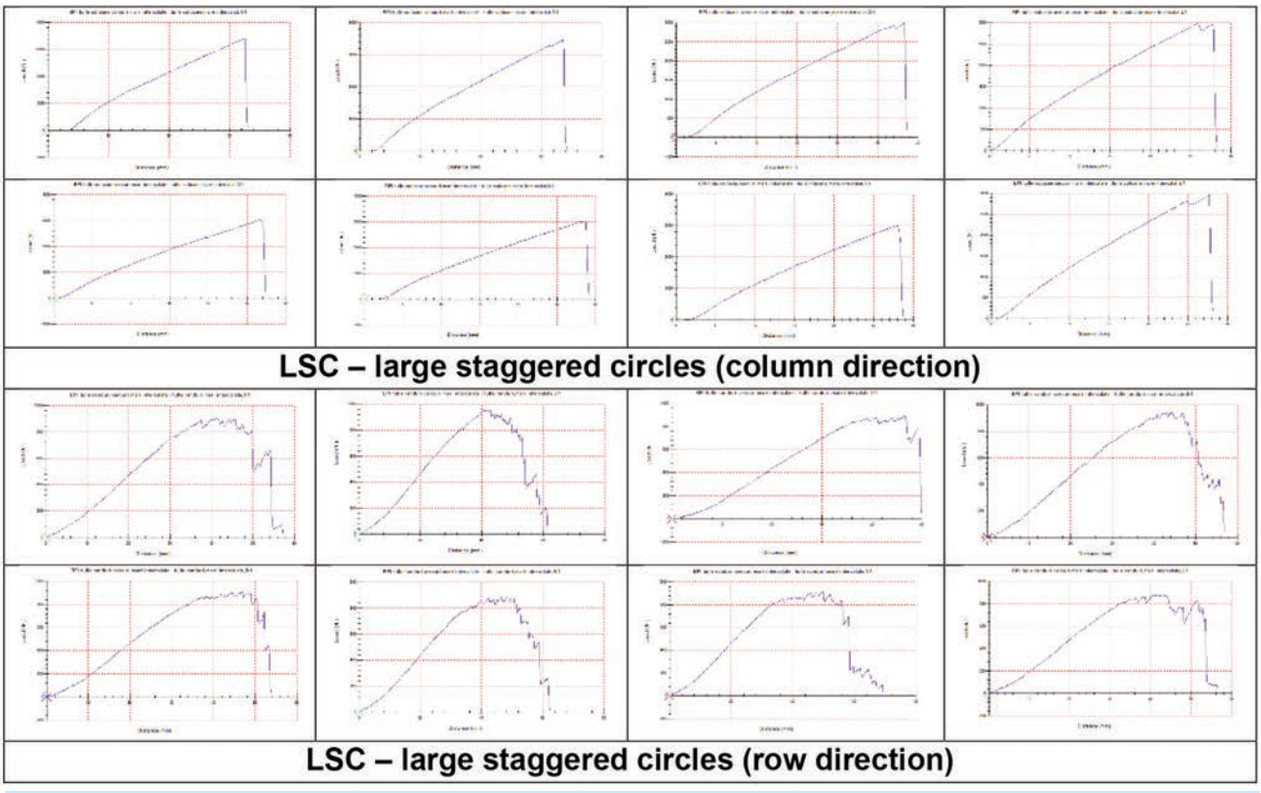


Fig. 12. The load-distance (force-extension) graphs for the LSC – Large Staggered Circles samples (Column/row direction)

behaviour and jagged descent patterns, suggesting progressive fibre and bond failures. Post-peak regions are more fragmented than in SAC or SSC, with multiple load drops, indicating micro-failure events and partial detachment or tearing within the printed pattern. The curves show lower slopes, indicative of lower stiffness and greater elongation in the column direction, but are more variable than SSC. The large ring pattern does not perform as well in the row direction, possibly due to misalignment between the load paths and the ring orientation, leading to localised stress concentrations. Fracture progression is more ductile, but less controlled, with evidence of crack propagation through the PLA network and tulle backing. The broader openings between rings may lead to stress localisation at fewer contact points, accelerating failure under crosswise strain.

LAC performs strongly in the warp direction, offering high strength but reduced ductility due to rigid geometric constraints. In the weft direction, the exact geometry becomes a structural weakness, as larger printed gaps and a mismatch in ring orientation hinder uniform force transfer. Compared to SAC and SSC, LAC is best used where directional strength is prioritised over overall flexibility.

All the LSC, Large Staggered Circles (column direction), curves show a relatively linear elastic phase, followed by a sharp peak and sudden drop, indicative of brittle-like failure (figure 12). Compared to small-circle models, the slope is more moderate, reflecting lower stiffness. Despite the reduced modulus, maximum load values remain high and consistent across samples. Minimal fluctuation in the post-peak region suggests a clean rupture without progressive tearing or delamination. The staggered pattern provides a balanced stress distribution, even in large-circle geometry, helping to delay rupture under uniaxial tensile force. However, the lower elastic modulus means deformation occurs more easily, which may be favourable for applications that need moderate flexibility with enhanced load capacity. The clean fracture profile indicates that while deformation occurs, the rupture is sudden and decisive, likely along predictable stress paths created by ring alignment.

For the LSC – Large Staggered Circles (row direction), the curves show a gradual rise to a peak, followed by a jagged, noisy decline, with many exhibiting plateau regions and stepped drops. This is characteristic of progressive micro-failure events, where the structure fails gradually rather than catastrophically. Slight undulations before the peak suggest internal redistribution of stress as some bonds yield before total rupture. The maximum force is lower than in the column direction, but relatively high compared to other row-direction models. In the weft direction, the large, staggered circles allow localised deformation and energy absorption, explaining the ductile behaviour observed in the force–distance graphs. The staggered layout helps to avoid abrupt stress concentrations, contributing to more controlled failure progression. This pattern shows promise in transverse reinforcement, where distributed performance and damage tolerance are needed.

Overall, the LSC geometry achieves a good compromise between strength and flexibility. It behaves predictably in the warp direction (sudden, high-load

rupture) and gracefully in the weft direction, where its staggered layout buffers crack propagation. This configuration may be best suited for applications requiring resilience and progressive energy dissipation, especially in multi-axial load environments.

The experimental results demonstrate a clear reinforcement effect induced by the 3D-printed circular patterns. Compared to unmodified tulle samples, all printed configurations exhibited increased maximum force and breaking strength, confirming effective stress transfer between the polymeric elements and the textile substrate.

This behaviour is consistent with findings reported in previous studies on textile–polymer hybrid structures, in which the printed material acts as a reinforcing phase [5, 16]. The adhesion between the polymer and textile enables load redistribution, leading to improved tensile performance.

However, the increase in strength is accompanied by a reduction in elongation at break, particularly in the weft direction. This effect can be attributed to the restriction of yarn mobility caused by the printed patterns, which limit the inherent deformability of the textile structure. Similar trade-offs between stiffness and flexibility have been observed in comparable additive manufacturing applications on textiles.

The results obtained in this study highlight the potential of additive manufacturing for the functional customisation of textile materials. By varying the size, spacing, and arrangement of printed elements, it is possible to locally tailor the mechanical properties of fabrics.

The ability to control stiffness and strength through geometric parameters enables the development of hybrid structures with spatially differentiated behaviour. This is particularly relevant in applications requiring localised reinforcement without compromising the overall flexibility of the material.

CONCLUSION

This study investigated the mechanical behaviour of a 3D-printed polymer layer deposited on a tulle fabric substrate, focusing on the influence of pattern geometry (aligned vs. staggered circles, small vs. large) and loading direction (warp vs. weft). Through uniaxial tensile tests and detailed visual and graphical analysis, several meaningful insights were drawn regarding the composite's structural performance.

Firstly, the presence of a 3D-printed pattern notably modified the mechanical properties of the tulle substrate. While the control samples (unprinted tulle) exhibited the highest elasticity and Young's modulus, especially in the weft direction, most printed samples showed reduced elongation and stiffness, indicating that the printed layer constrains the native deformability of the textile mesh. Despite this reduction in flexibility, all printed configurations demonstrated higher maximum force and breaking strength than the control, particularly in the column (warp) direction. This reveals the reinforcing effect of the polymeric overlay, which shares the tensile load and delays failure.

Among the printed geometries, small aligned and staggered circles (SAC and SSC) proved more effective in maintaining balanced mechanical performance, offering moderate flexibility while significantly improving strength. In contrast, large patterns, particularly those aligned (LAC), although providing higher force resistance, induced stress concentration zones at the edges, which occasionally led to premature and irregular failure, especially in the row (weft) direction. The staggered large-circle configuration (LSC) displayed interesting ductile behaviour with multiple load peaks before rupture, suggesting progressive failure mechanisms and partial energy dissipation within the network.

The fracture zones of most samples occurred near the clamping edge, an expected deviation for highly porous textiles like tulle, due to localised stress concentrations and mesh deformation under pressure. This phenomenon was observed consistently across all specimen types and directions, reinforcing the validity of relative comparisons across sample groups.

Force-elongation curves further confirmed these conclusions: control samples exhibited smooth, long curves indicating elastic deformation, while printed samples demonstrated sharper transitions, sudden drops (linked to partial delamination or rupture of the printed layer), and shorter extension paths, consistent with their reduced ductility.

In sum, 3D printing directly on textiles creates a new class of hybrid materials whose mechanical behaviour can be finely tuned by adjusting pattern geometry and orientation. The directionality of the textile plays a crucial role, as the warp (column) direction inherently offers higher stiffness and load-bearing capacity. The study confirms the potential of fused deposition modelling (FDM) to enhance or customise the performance of lightweight fabrics such as tulle, paving the way for applications in wearable technology, smart textiles, and functional garment engineering.

The findings of this study demonstrate that 3D-printed circular patterns can effectively modify the tensile behaviour of lightweight textile substrates such as tulle. The influence of pattern size and arrangement plays a critical role in determining the balance between strength and flexibility.

These results open new perspectives for applications in:

- fashion design, where structural reinforcement can be integrated into garments;
- technical textiles, requiring localised mechanical enhancement;
- wearable technologies, where printed elements can support embedded components;
- medical textiles, including customised orthotic and support systems.

Future work will focus on multi-material printing, adaptive geometries, and the integration of functional elements to further enhance the performance of textile–polymer composite systems.

Future research could explore the use of different filament materials (flexible or conductive), multilayered patterns, or multi-material strategies to optimise both mechanical and functional characteristics in line with specific end-use requirements.

ACKNOWLEDGEMENT

This work was supported by Craft Revitalisation Action for Future-proofing the Transition to Innovative Technologies for Sustainable Development – CRAFT-IT4SD/no. 101132596/ HORIZON-CL2-2023-HERITAGE-01.

REFERENCES

[1] Keefe, E.M., Thomas, J.A., Buller, G.A., Banks, C.E., *Textile additive manufacturing: An overview*, In: Cogent Engineering, 2022, 9, 1, 2048439, https://doi.org/10.1080/23311916.2022.2048439

[2] Chakraborty, N., Biswas, D., *Additive technologies in apparel engineering*, In: Journal of Textile Engineering, 2020, 66, 3, 45–58

[3] Sanatgar, R.H., Campagne, C., Nierstrasz, V., *Investigation of adhesion in direct 3D printing of polymers and nanocomposites on textiles,* In: Applied Surface Science, 2017, 403, 551–563, https://doi.org/10.1016/j.apsusc.2017.01.112

[4] Gorlachova, M., Mahltig, B., *3D-printing on textiles – an investigation on adhesion properties of the produced composite materials,* In: Journal of Polymer Research, 2021, 28, 1–10, https://doi.org/10.1007/s10965-021-02567-1

[5] Fajardo, J.I., Farez, M.V., Paltán, C.A., *Experimental analysis of the relationship between textile structure, tensile strength and comfort in 3D printed structured fabrics*, In: Polymers, 2023, 15, 1, 152, https://doi.org/10.3390/polym15010152

[6] Yang, L., Li, N., Fang, J., Zhang, X., *Auxetic metamaterials fabricated by additive manufacturing: A review*, In: Materials & Design, 2020, 195, 109034

[7] Valtas, A., Sun, D., *3D printing for garment production: An exploratory study*, In: Journal of Fashion Technology & Textile Engineering, 2016, 4, 3, 2329

[8] Mpofu, N., Marecha, A., Mvubu, M., *Effects of FDM parameters on adhesion of PLA to polyester textiles*, In: Journal of Engineered Fibres and Fabrics, 2020, 15, 1–10

[9] Grimmelsmann, N., Kreuziger, M., Korger, M., Lutz, M., Ehrmann, A., *Adhesion of 3D printed material on textile substrates*, In: Proceedings of the 2016 International Textile Conference, 2016, 152–158

[10] Chen, X., Li, X., Kuk, D., Xu, W., *All-fabric triboelectric e-skin for tactile sensing textiles*, In: Nano Energy, 2021, 89, 106–113

[11] Passlack, P., Potthast, S., Yilmaz, E., *Additive manufacturing of decorative textile surfaces,* In: Rapid Prototyping Journal, 2013, 19, 2, 129–136

[12] Richter, D., Schmied, A., Wessel, R., *Additive manufacturing of floral patterns on textiles*, In: Rapid Prototyping Journal, 2015, 21, 3, 207–214

[13] Kozior, T., Blachowicz, T., Ehrmann, A., *Adhesion of three-dimensional printing on textile fabrics: Inspiration from and for other research areas*, In: Journal of Engineered Fibers and Fabrics, 2020, 15, 1–11, https://doi.org/10.1177/1558925020910875

[14] Korger, H., Bergschneider, J., Lutz, M., Mahltig, B., Finsterbusch, K., Rabe, M., *Possible applications of 3D printing technology on textile substrates*, In: IOP Conference Series: Materials Science and Engineering, 2016, 141, 012011, https://doi.org/10.1088/1757-899X/141/1/012011

[15] Robinson, B., Imam, A., Sabir, T., Ahmed, A., *Application of additive manufacturing on textiles,* In: TIWC Conference Proceedings, 2024, 1–14

[16] Sabantina, L., Kinzel, F., Ehrmann, A., Finsterbusch, K., *Combining 3D printed forms with textile structures*, In: IOP Conference Series: Materials Science and Engineering, 2015, 87, 012005, https://doi.org/10.1088/1757-899X/87/1/012005

[17] Ren, X., Das, R., Tran, P., Ngo, T., *Mechanical behavior of chiral and auxetic structures manufactured via additive techniques*, In: Additive Manufacturing, 2021, 38, 101839

[18] Crump, S., *Apparatus and method for creating three-dimensional objects*, US Patent No. 5121329, 1989

[19] Ghafar, A., Riaz, M.T., Rehman, A., Al-Mahmud, M.M.S., *An Optimized 3D Printer by Enhancing Material Properties and Surface Finish of PLA Through Modifications*, In: Journal of Engineering, 2024, 1, 9198329, 1–12, https://doi.org/10.1155/2024/9198329

[20] Gkertzos, P., Kotzakolios, A., Mantzouranis, G., Kostopoulos, V., *Nozzle Temperature Calibration in 3D Printing: Environmental Implications for Material Quality and Adhesion*, In: IOP Conference Series: Materials Science and Engineering, 2024, 1388, 012012, 1–10, https://doi.org/10.1088/1757-899X/1388/1/012012

[21] Parajuli, D., Acharya, S., Sedhain, R., Joshi, R., *The evolution of textile fibers and modern sustainable materials*, In: Fibers, 2021, 9, 2, 1–14

[22] Stratasys Ltd., *Textile-Focused Additive Manufacturing Systems: Product Overview. Stratasys Technical Publication*, 2023, Available at: https://www.stratasys.com [Accessed on December 6, 2025]

[23] Thumsorn, S., Mongkholrattanasit, R. & Ruckdashel, R., *Influence of thermal conditions on interlayer bonding and mechanical properties in FDM printing*, In: Polymer Testing, 2023, 125, 108153, https://doi.org/10.1016/j.polymertesting.2023.108153

[24] Ren, Z., Jiang, J., Smith, C., *Energy absorption characteristics of additively manufactured cellular structures: A review*, In: Materials & Design, 2020, 194, 108890, https://doi.org/10.1016/j.matdes.2020.108890

[25] Rusu, P.-D., *Characterization of Laser-Textured Surfaces – A Review*, In: Buletinul Institutului Politehnic din Iași, Section: Materials Science and Engineering, 2025, 71, 75/2, 9–28

[26] Sabir, T., Imam, A., *Optimising 3D-Printed Metamaterial Patterns for Fabric–Polymer Bond Strength*, In: Proceedings of the Textiles Innovation and Wearable Computing (TIWC) Conference, Canterbury Christ Church University / Manchester Metropolitan University, 2024, 1–12

[27] Avadanei, M.L., Olaru, S., Dulgheriu, I., Ionesi, S.D., Loghin, E.C., Ionescu, I., *A New Approach to Dynamic Anthropometry for the Ergonomic Design of a Fashionable Personalised Garment*, In: Sustainability, 2022, 14, 13, https://doi.org/10.3390/su14137602

[28] Gavancho, J.R.F., Condori, V.M.L., Mamani, S.Q., Mamani, U.Q., Yépez, J.J.V., Robles, R.T., *Evaluation of wash colour strength of a printed garment with flexible filaments on 3D printers*, In: Industria Textila, 2024, 75, 5, 556–564, http://doi.org/10.35530/IT.075.05.2023100

[29] *ISO 13934-1: Textiles. Tensile properties of fabrics. Part 1: Determination of maximum force and elongation at maximum force using the strip method*, Available at: https://www.iso.org/obp/ui/en/#iso:std:iso:13934:-1:ed-2:v1:en [Accessed on December 4, 2025]

[30] *ISO 1421: Rubber- or plastics-coated fabrics. Determination of tensile strength and elongation*, Available at: https://www.iso.org/obp/ui/en/#iso:std:iso:1421:ed-3:v1:en [Accessed on December 4, 2025]

Authors:

IULIANA STREBA[1], ARINA SEUL[1,2], AURA MIHAI[1,2], ANTONELA CURTEZA[1], MARIANA COSTEA[1,2], RAMONA BUDEANU[1,2]

[1]"Gheorghe Asachi" Technical University of Iasi, Faculty of Industrial Design and Business Management, 29 Prof. Dr. Docent D. Mangeron Blvd, 700050-Iasi, Romania

[2]Centre for Research and Innovation in Textiles and Fashion Industry – SMART-Tex-IS, str. Prof. Dr. Doc. Dimitrie Mangeron, 29, Iași, 700050

Corresponding author:

MARIANA COSTEA
e-mail: mariana.costea@academic.tuiasi.ro